On-Demand Bulk Nanobubble Generation through Pulsed Laser Illumination

Juan Manuel Rosselló and Claus-Dieter Ohl
Otto von Guericke University Magdeburg, Institute of Experimental Physics,
Universitätsplatz 2, 39106 Magdeburg, Germany

We demonstrate the temporally and spatially controlled nucleation of bulk nanobubbles in water through pulsed laser irradiation with a collimated beam. Transient bubbles appear within the light exposed region once a tension wave passes through. The correlation between illumination and cavitation nucleation provides evidence that gaseous nanobubbles are nucleated in the liquid by a laser pulse with an intensity above 58 MW/cm^2. We estimate the radius of the nanobubbles through microscopic high-speed imaging and by solving the diffusion equation to be below 420 nm for $\sim$80% of the bubble population. This technique may provide a novel approach to test theories on existence of stable bulk nanobubbles.

Introduction.—In the last decade the interest in the stable encapsulation of gas by submicron-sized bubbles in water grew considerably. Because of their small size these so-called bulk nanobubbles although buoyant may remain stably suspended. This interest was stimulated by a diverse range of potential applications in areas such as waste treatment, cleaning and purification technologies, in biomedicine, food processing, and sonochemistry [1–5]. Additionally, the existence of such bulk nanobubbles would have an impact on marine aquatic life and for the delivery of oxygen to livestock in aquacultures [6]. A number of methods for nanobubble generation have been reported. These include repeated and controlled liquid pressure variations [7–9], mechanical agitation [10], ultrasound irradiation [11], electrolysis [12], or oversaturation of liquids through the mixing of alcohols with water [13,14]. While the number of studies utilizing nanobubbles in research has increased dramatically, very few of these deal with confirming their gaseous nature. In nearly all research papers the size distribution of the bulk nanobubbles is obtained from laser scattering, i.e., nanoparticle tracking and dynamic light scattering [8,12,13,15]. The danger stemming from these kinds of measurements is their blindness to the very nature of the scattering objects and thus they could easily be confused with pollutant droplets or nanoparticles [10,14,16,17]. This missing confirmatory assessment in published research on nanobubbles leads to considerable discussion on their existence, e.g., see Refs. [9,18–20].

In the present approach, unambiguous evidence for the on-demand generation of gaseous submicron sized bubbles is provided. The method is as simple as shining a moderately intense and collimated laser beam through a cuvette filled with deionized water. While the bubbles are generated during the laser beam passage, they remain for several tens of milliseconds in the liquid. The laser pulse intensity was about at least 2 orders of magnitude smaller than the reported intensity threshold for multiphoton ionization of water at 532 nm of $I_{\text{thres}} = 30$ GW/cm^2 [1,21,22]. At this wavelength light passes practically without absorption through water and no particles were added that may lead to short short-lived cavitation bubbles, e.g., through a plasmonic resonance [15,23–26]. While the mechanism of nanobubble generation is not understood, their presence and gaseous nature is revealed by passing a rarefaction wave through the illuminated volume.

Experimental methods.—The experimental setup is sketched in Fig. 1 (more details are provided in the Supplemental Material [27]). In short, the collimated 800 μm beam of the nanobubble "seeding" laser (*Litron Nano T-250-10*; $\lambda = 532$ nm; FHMW $= 7$ ns) passes through the water at a depth of $\sim$1 mm parallel to its surface with a pulse energy of $\sim$8 mJ. The deionized and filtered water (200 nm PTFE membrane, $\sim$1 MΩ cm resistivity) is contained in a glass cuvette with square cross section (1 cm width, 5 cm height). To detect gaseous bubbles below the optical resolution limit, we utilize a rarefaction wave passing through the laser exposed volume. Thereby forcing their expansion and making them visible. The rarefaction is generated with a second laser pulse (*Litron Nano SG-100-2*; $\lambda = 532$ nm; FHMW $= 6$ ns, pulse energy $\sim$5 mJ) that is focused with a 20$\times$ microscope objective ($f = 15$ mm; NA $= 0.33$) near to the liquid surface (typically 200 μm below) resulting in a dielectric breakdown. Consequently, a shock wave is emitted that upon reflection at the free surface results in a trailing rarefaction wave. The liquid is therefore exposed to a bipolar pressure transient, that starts with a positive pressure from the initial shock wave followed by a negative pressure peak (see Fig. 1). The delay Δt between the illuminating laser pulse to seed the nanobubbles and the laser pulse generating the tension wave is adjustable.
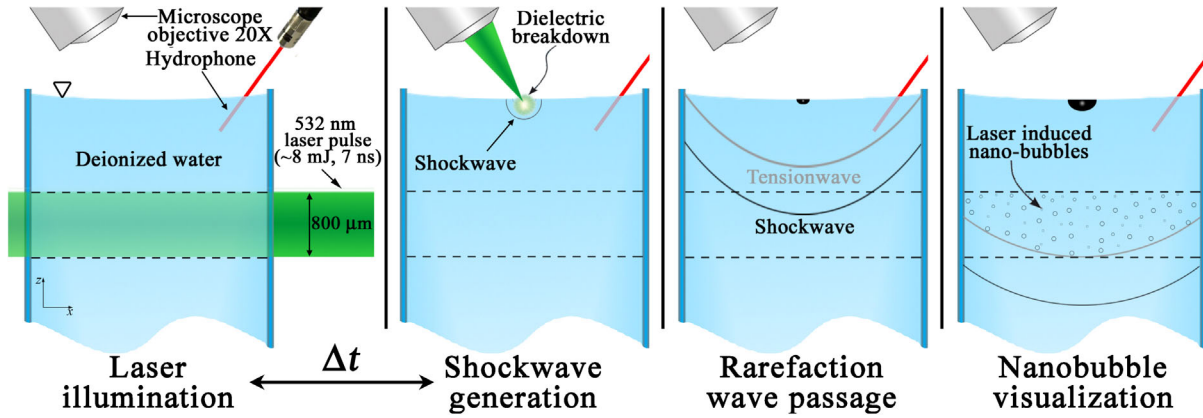
FIG. 1.   Sketch of the experimental method. The nanobubbles are generated by a short and collimated laser pulse illuminating the water. A shock wave is generated after a time Δt focusing a second laser pulse close to the liquid surface, that is reflected at the free surface as a rarefaction wave. Once the rarefaction wave has traveled through the illuminated volume, the nanoscopic gaseous voids are expanded and become visible with optical microscopy.

The bubble dynamics in the liquid is captured with a high-speed camera at a frame rate of 5 Mfps (*XPV-X2, Shimadzu*). In order to obtain sharp images of the acoustic waves and the rapid bubble dynamics, we implemented a backlight illumination from a pulsed femtosecond laser (*Ekspla FemtoLux 3*, $\lambda = 515$ nm) emitting ultrashort pulses (230 fs) at a frequency of 5 MHz, i.e., at the same rate as the camera records the frames. Different image magnifications were achieved with a selection of long distance microscope objectives (*Edmund Optics*) with 5×, 10×, 20×, or 50×. Those were complemented with protective notch filters and a second macrolens (*macrolens LAOWA f2.8*) with a variable magnification of up to 2×. This optical arrangement in combination with the 400×250 pixels of the high speed camera sensor results in an imaging resolution ranging between 7 μm/px and 230 nm/px.

The pressure profile of the bipolar transient wave was measured with a fiber optic hydrophone *Onda HFO-690*

with a spatial resolution of 100 μm and stored with a sampling rate of 20 GSa/s (analog bandwidth 4 GHz). We obtained over 175 measurements 8.0 ± 0.2 MPa for the positive peak and -5.2 ± 0.2 MPa of negative pressure peak in the rarefaction wave. Both extreme values show a standard deviation of $\sim$2 MPa. We explain this variation with the sensitivity of the shock wave strength to slight variations of the water height and thus the depth of the focusing of the "shock" laser pulse. The delay between the seeding laser pulse and the shock laser pulse was controlled with a digital delay generator *Quantum 9520*. A jitter of around 100 ns was found in the arrival time of the bipolar wave.

Results and discussion.—A typical experiment is presented in Fig. 2: At time $t = 0$ the collimated laser beam passes between the two indicated boundaries [dashed line in Fig. 2(a)] through the liquid filled cuvette. At the same time (i.e., $\Delta t = 0$), the bipolar pulse is generated 200 μm below the liquid surface and about 1 mm away from the
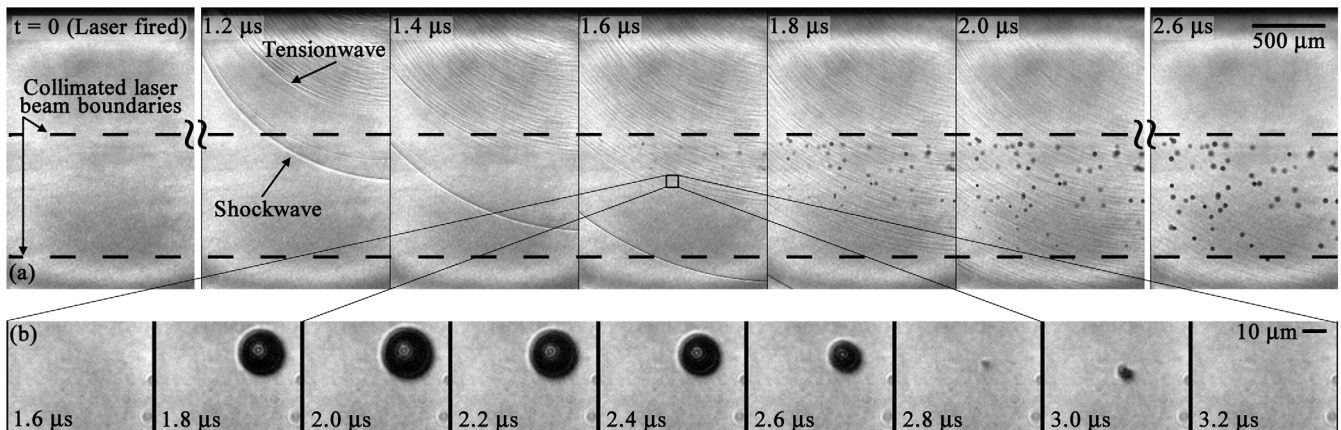
FIG. 2.   Laser induced nanobubble cloud. The times in the figure are relative to the firing of the seeding laser. (a) No bubbles are observed outside the seeding laser beam path (800 μm) indicated by the dashed lines. (b) Detail of a typical nanobubble dynamics captured with an optical resolution of 234 nm/px. The bubble size is below the optical resolution prior and after the expansion-collapse cycle. See Supplemental Material [27] for a more detailed sequence.

upper dashed boundary. Until $t < 1.4\,\mu$s the volume through which the laser pulse has passed remains void of objects besides the waves visualized by means of the short illumination pulses. At $t = 1.6\,\mu$s bubble nucleation sets in, trailing rather homogeneously the rarefaction wave, yet only within the boundaries of the collimated laser beam as indicated by the dashed lines in Fig. 2(a).

The experiment provides two clear findings. First, the laser pulse is creating invisible gas bubbles that are expanded by the tension wave resulting in visible bubbles appearing within the volume of the illuminated region. Second, as the strength of the tension wave decays with distance, the liquid above the illuminated region is exposed to a stronger tensile amplitude than the laser illuminated volume below. Thus, we can rule out acoustic cavitation from naturally existing nuclei in the water generated by the tension wave. This was further tested by conducting control measurements where no collimated laser was fired. In those, we did not observe cavitation within the field of view. This second test is important as the focused shock laser pulse may generate gaseous fragments through the later collapse of a cavitation bubble near the free surface. Furthermore, as bubbles are only nucleated between the dashed lines we can exclude any transported cavitation nuclei into the field of view of Fig. 2(a).

Figure 2(b) depicts selected frames from a recording taken within the indicated region of Fig. 2(a) at a higher magnification with a pixel resolution of 234 nm/px from a different experimental run. For times $t <= 1.6\,\mu$s no objects are discernible from the frames background. Between $1.6\,\mu$s $< t < 1.8\,\mu$s a bubble expands explosively to $R = 10.7 \pm 0.3\,\mu$m, reaches a maximum radius as $t = 2.0\,\mu$s and collapses at $t = 2.8\,\mu$s. The reexpansion at $t = 3.0\,\mu$s is evidence of some nonspherical shape. After $t > 3.0\,\mu$s the bubble is again not discernible from the background. During the first expansion the bubble will collect gas by rectified diffusion. Equating this amount of gas influx with the volume of a bubble at rest results in a bubble radius of $\sim$220 nm [30]. As the dissolution time of a bubble slightly larger than this size is considerably longer than the interframe time of 200 ns, we can give a lower bound of the optical resolution of 500 nm. Bubbles that are expanding to a larger maximum radius may remain barely noticeable as a moving shady spot. In those particular cases, their estimated rest radius including the growth due to rectified diffusion is about 500 nm (See Supplemental Material [27] for multimedia visualization). This observation agrees with the expected effective optical resolution of the setup for an illumination wavelength of $\lambda = 515$ nm and numerical aperture NA $= 0.42$.

In spite of the high spatial and temporal resolution achieved in these measurements, the origin of the bubbles is not clear. No colloidal particles in the liquid or visible plasma spots were observed (even when recording the videos without the backlight illumination).

The reported generation of gaseous cavitation nuclei can be connected to previous observation of secondary cavitation where the laser pulse was tightly focused to create optic cavitation. Already in 1974, Lauterborn noted the creation of secondary cavitation bubbles on the sides of the laser focus in water at reduced static pressure [31,32]. Very recently the formation of bubbles along a focused laser beam path was reported by Požar *et al.* [33] and connected with acoustic cavitation due to a tension wave. This may also be the explanation for the secondary cavitation seen after focusing a rather intense laser pulses close to a free surface [34,35]. We are aware of only one work that demonstrates the nucleation of cavitation nuclei from a nonfocused laser pulse in a phosphoric acid aqueous solution [36]. Here a continuous acoustic field expands the bubbles to visible size.

The degree of control over the bubble production using a laser seeding technique is advantageous over the earlier mentioned methods of sudden decompression, liquid shaking, ultrasound, or electrolysis. Here, the liquid volume and the number of bubbles can be controlled with a simple optical system and by adjusting the intensity of the laser beam [37,38]. In our experiment, the seeding threshold intensity was approximately 58 ± 10 MW/cm^2. This intensity is about 500 times smaller than the reported intensity threshold for optical breakdown [21,22].

Let us now compare the measured bubble dynamics with a suitable spherical bubble model, for example the Keller-Miksis model [39,40]. Therefore we use the hydrophone measurement to drive a seed bubble nucleus with an initial size R_0 that is below the optical resolution and compare the obtained radial dynamics with one extracted from the high-speed recording. The bipolar driving pressure is shown in the upper graph of Fig. 3 and next to it a picture from the very same experiment showing the position of the hydrophone, the illuminating light diffracted by the spherical pressure wave, and the first visible image of the bubble generated in the tensile region of the wave.

We obtain good agreement between the predicted bubble dynamics and the measured expansion of the bubble for the first oscillation cycle of a bubble with $R_0 = 60$ nm. Interestingly, during the rebound the bubble expands distorted and also slightly shifted from its original location (See Supplemental Material [27] for details). As the Keller-Miksis (KM) model does not include translation motion or nonspherical bubble dynamics we limit the simulations up to the first collapse.

Additionally, Fig. 3 shows the dynamics of bubbles of different initial size R_0. The simulated results reveal that there is a limit on the size of the bubbles that the tension wave can expand, and, consequently, be observed using the method proposed in this work. To learn more about this matter a parametric numerical analysis was conducted. In the latter, the ambient radius R_0 and the amplitude of the tension wave were varied and plotted against the maximum
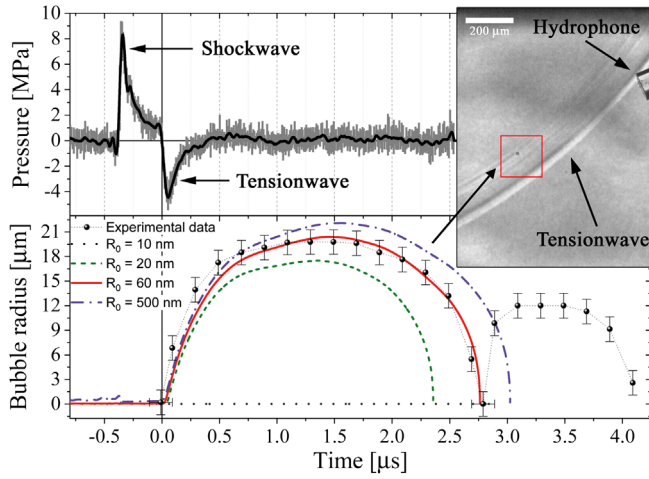
FIG. 3. Detail of the dynamics of a nanobubble. The bubble radius temporal evolution $[R(t)]$ is obtained from the video frames (graph inset). A smoothed trace of the pressure variation recorded by the hydrophone (black line) was used as the driving pressure in the numerical fit (red line) of the measured $R(t)$. The best fit was obtained for an ambient radius of $R_0 = 60$ nm. The measured rebound of the bubble after the collapse is dramatically affected by the water volume entering the gas cavity during the jetting [41]. See Supplemental Material [27] for the complete image sequence.

radius reached by the bubble on each case (see Supplemental Material [27] for details). As a result we find that for an amplitude of -5 MPa of the rarefaction wave and considering a limit in the observable radius of 4 μm [similar to the pixel resolution of Fig. 2(a)], nanobubbles down to an initial radius of $R_0 \geq 15$ nm can be detected. Examples of bubbles with larger and smaller size are compared with the measurement in Fig. 3 (and also in the Supplemental Material [27]). While a bubble with 10 nm in radius hardly responds to the pressure variation [42], a bubble of 500 nm initial radius shows a very similar behaviour as the best fit of 60 nm.

Although a numerical fit with the Keller-Miksis equation provides a robust method to account of the nanometric scale of the bubbles [43], it is important to note that this method might be not suitable for all the bubbles composing of the bubble clusters. Specifically, the KM model applies to cases where the interaction between bubbles can be neglected and the hydrophone is sufficiently close to the imaged bubble to obtain an accurate pressure or tension trace. Then, a characterization of the complete bubble size distribution (at a given time Δt) would require more sophisticated models (and maybe measurements) than the one used here.

An alternative way to estimate the initial size of the gas nuclei is through the measurement of its lifetime until their dissolution. In the absence of any stabilizing mechanisms, e.g., Ref. [20], the bubble will shrink to zero size due to the higher gas pressure in the bubble as compared to partial pressure in the liquid. The Epstein-Plesset model has
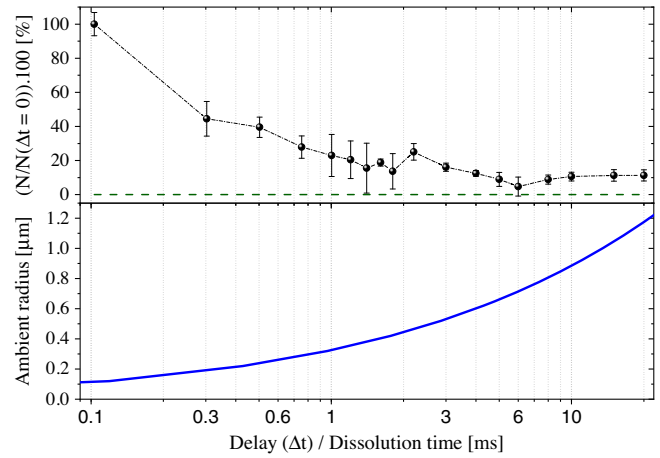
FIG. 4. *Top*: Percentage of nanobubbles present in the solution as a function of the time Δt between seeding and observation, $N(\Delta t \to 0) \simeq 112$ [within the ROI in Fig. 2(a)]. The mean amplitude of the tension wave is -5.0 ± 0.2 MPa. The dashed horizontal line indicates the mean bubble number in absence of bubble seeding. *Bottom*: Bubble lifetime as a function of the initial bubble radius according to the Epstein-Plesset model. The dissolution times found indicate that most of the nucleated bubbles have ambient radius below 400 nm.

successfully been used to described the dissolution of bubbles optically down to a size of 1 μm [44].

In the experiment, this stabilization was tested by counting the bubble number captured in the videos while varying the delay Δt between the seeding laser pulse and the tension wave arrival. Figure 4 shows the average bubble population detected for values of Δt up to 20 ms, along with a numerical calculation of the bubble dissolution time performed with the Epstein-Plesset theory [45]. The computations were carried out considering air saturated water at standard ambient temperature and pressure (i.e., $T = 293$ K and $P_0 = 101.3$ kPa, respectively). The air-liquid surface tension was $\sigma = 0.072$ J/m^2, the gas density was $\rho_g = 1.2$ kg/m^3, the diffusion coefficient $D = 1.9 \times 10^{-9}$ m^2/s, and the saturation concentration of air in water was taken as $c_{\text{sat}} = 0.0227$ g/l).

Figure 4 shows how the bubble population is significantly reduced within the first millisecond after their inception. According to Epstein-Plesset theory, 80% of the bubbles should have had an initial (seeding) radius below 400 nm. In the same way, it is possible to see that 60% of the bubbles disappear during the first 500 μs after the seeding, which implies that most of the bubbles have ambient radius under 220 nm. The bubble sizes estimated in this way are in perfect agreement with the limit values inferred from the videos. The few bubbles that have not dissolved after 20 ms may either be the result of seeding of bubbles above 1.2 μm in radius and/or are the result of some stabilization of bulk nanobubbles.

Conclusion and outlook.—We have demonstrated the production of bulk nanobubbles with ambient radii below

500 nm through the passage of an intense laser pulse in water and confirmed their gaseous nature unambiguously. Unfortunately, the seeding mechanism could not be clarified, yet the absence of plasma hot spots suggests some absorption of energy likely from particles or liquid contamination in the water. The nanobubbles are generated on demand and localized along the optical path. This is a clear advantage to the nanobubble production techniques reported previously [7–14]. In the experiments, the short exposure times of the high-speed images were crucial to capture the shock waves and the microscopic bubble dynamics without motion blurring. With the availability of this controlled nanobubble generation technique reproducibility issues plaguing the research field can now be addressed. As a first utilization we suggest to analyze the effect of liquid properties on the lifetime of nanobubbles, e.g., the pH level and the liquid temperature [20,45,46]. The direct visualization of the nanobubbles opens the possibility of a reliable study on how nanobubbles can be stabilized in solution. The latter can be complemented with fast light scattering techniques, e.g., based on high-speed imaging [47] to resolve the bubble size distribution below the optical limit.

[1] A. Vogel, N. Linz, S. Freidank, and G. Paltauf, Femtosecond-Laser-Induced Nanocavitation in Water: Implications for Optical Breakdown Threshold and Cell Surgery, Phys. Rev. Lett. 100, 038102 (2008).

[2] M. Alheshibri, J. Qian, M. Jehannin, and V. S. J. Craig, A history of nanobubbles, Langmuir 32, 11086 (2016).

[3] T. Temesgen, T. T. Bui, M. Han, T.-I. Kim, and H. Park, Micro and nanobubble technologies as a new horizon for water-treatment techniques: A review, Adv. Colloid Interface Sci. 246, 40 (2017).

[4] S. Haris, X. Qiu, H. Klammler, and M. M. Mohamed, The use of micro-nano bubbles in groundwater remediation: A comprehensive review, Groundw. Sustain. Dev. 11, 100463 (2020).

[5] K. K. Thi Phan, T. Truong, Y. Wang, and B. Bhandari, Nanobubbles: Fundamental characteristics and applications in food processing, Trends Food Sci. Technol. 95, 118 (2020).

[6] K. Ebina, K. Shi, M. Hirao, J. Hashimoto, Y. Kawato, S. Kaneshiro, T. Morimoto, K. Koizumi, and H. Yoshikawa, Oxygen and air nanobubble water solution promote the growth of plants, fishes, and mice, PLoS One 8, 2 (2013).

[7] Q. Wang, H. Zhao, N. Qi, Y. Qin, X. Zhang, and Y. Li, Generation and stability of size-adjustable bulk nanobubbles based on periodic pressure change, Sci. Rep. 9, 1 (2019).

[8] G. Ferraro, A. J. Jadhav, and M. Barigou, A Henry's law method for generating bulk nanobubbles, Nanoscale 12, 15869 (2020).

[9] A. J. Jadhav and M. Barigou, Bulk nanobubbles or not nanobubbles: That is the question, Langmuir 36, 1699 (2020).

[10] S. H. Oh and J.-M. Kim, Generation and stability of bulk nanobubbles, Langmuir 33, 3818 (2017).

[11] K. Yasuda, H. Matsushima, and Y. Asakura, Generation and reduction of bulk nanobubbles by ultrasonic irradiation, Chem. Eng. Sci. 195, 455 (2019).

[12] K. Kikuchi, A. Ioka, T. Oku, Y. Tanaka, Y. Saihara, and Z. Ogumi, Concentration determination of oxygen nanobubbles in electrolyzed water, J. Colloid Interface Sci. 329, 306 (2009).

[13] J. Qiu, Z. Zou, S. Wang, X. Wang, L. Wang, Y. Dong, H. Zhao, L. Zhang, and J. Hu, Formation and stability of bulk nanobubbles generated by ethanol water exchange, ChemPhysChem 18, 1345 (2017).

[14] F. Eklund, M. Alheshibri, and J. Swenson, Differentiating bulk nanobubbles from nanodroplets and nanoparticles, Curr. Opin. Colloid Interface Sci. 53, 101427 (2021).

[15] R. Lachaine, É. Boulais, and M. Meunier, From thermo- to plasma-mediated ultrafast laser-induced plasmonic nanobubbles, ACS Photonics 1, 331 (2014).

[16] M. Alheshibri and V. S. J. Craig, Differentiating between nanoparticles and nanobubbles by evaluation of the compressibility and density of nanoparticles, J. Phys. Chem. C 122, 21998 (2018).

[17] D. Rak and M. Sedlák, Comment on "bulk nanobubbles or not nanobubbles: That is the question", Langmuir 36, 15618 (2020).

[18] N. Nirmalkar, A. W. Pacek, and M. Barigou, On the existence and stability of bulk nanobubbles, Langmuir 34, 10964 (2018).

[19] M. Alheshibri and V. S. Craig, Generation of nanoparticles upon mixing ethanol and water; Nanobubbles or Not?, J. Colloid Interface Sci. 542, 136 (2019).

[20] B. H. Tan, H. An, and C. D. Ohl, Stability of surface and bulk nanobubbles, Curr. Opin. Colloid Interface Sci. 53, 101428 (2021).

[21] A. Vogel, K. Nahen, D. Theisen, and J. Noack, Plasma formation in water by picosecond and nanosecond Nd:YAG laser pulses. I. Optical breakdown at threshold and superthreshold irradiance, IEEE J. Sel. Top. Quantum Electron. 2, 847 (1996).

[22] J. Noack and A. Vogel, Laser-induced plasma formation in water at nanosecond to femtosecond time scales: calculation of thresholds, absorption coefficients, and energy density, IEEE J. Quantum Electron. 35, 1156 (1999).

[23] D. Lapotko, Optical excitation and detection of vapor bubbles around plasmonic nanoparticles, Opt. Express 17, 2538 (2009).

[24] E. Lukianova-Hleb, Y. Hu, L. Latterini, L. Tarpani, S. Lee, R. A. Drezek, J. H. Hafner, and D. O. Lapotko, Plasmonic Nanobubbles as transient vapor nanobubbles generated around plasmonic nanoparticles, ACS Nano 4, 2109 (2010).

[25] R. Lachaine, E. Boulais, E. Bourbeau, and M. Meunier, Effect of pulse duration on plasmonic enhanced ultrafast laser-induced bubble generation in water, Appl. Phys. A **112,** 119 (2013).

[26] Y. Wang, M. E. Zaytsev, H. L. The, J. C. T. Eijkel, H. J. W. Zandvliet, X. Zhang, and D. Lohse, Vapor and gas-bubble growth dynamics around laser-irradiated, water-immersed plasmonic nanoparticles, ACS Nano **11,** 2045 (2017).

[27] See Supplemental Material at http://link.aps.org/supplemental/10.1103/PhysRevLett.127.044502 for a detailed description of the experimental setup and an extended discussion on the results. Additionally, the multimedia files corresponding to the measurements performed can be found in the link, which includes Refs. [28,29].

[28] S. W. Gong, S. W. Ohl, E. Klaseboer, and B. C. Khoo, Scaling law for bubbles induced by different external sources: Theoretical and experimental study, Phys. Rev. E **81,** 056317 (2010).

[29] G. Sinibaldi, A. Occhicone, F. Alves Pereira, D. Caprini, L. Marino, F. Michelotti, and C. M. Casciola, Laser induced cavitation: Plasma generation and breakdown shockwave, Phys. Fluids **31,** 103302 (2019).

[30] M. Arora, L. Junge, and C. Ohl, Cavitation cluster dynamics in shock-wave lithotripsy: Part 1. Free field, Ultrasound Med. Biol. **31,** 827 (2005).

[31] W. Lauterborn, Kavitation durch laserlicht, Acustica **31,** 51 (1974).

[32] W. Lauterborn, *Cavitation and Inhomogeneities in Underwater Acoustics*, edited by W. Lauterborn (Springer Berlin Heidelberg, Berlin, Heidelberg, 1980).

[33] T. Požar and R. Petkovšek, Cavitation induced by shock wave focusing in eye-like experimental configurations, Biomed. Opt. Express **11,** 432 (2020).

[34] P. Koukouvinis, M. Gavaises, O. Supponen, and M. Farhat, Simulation of bubble expansion and collapse in the vicinity of a free surface, Phys. Fluids **28,** 052103 (2016).

[35] O. Supponen, D. Obreschkow, P. Kobel, M. Tinguely, N. Dorsaz, and M. Farhat, Shock waves from nonspherical cavitation bubbles, Phys. Rev. Fluids **2,** 093601 (2017).

[36] J. M. Rosselló, D. S. Stephens, and R. Mettin, Bubble "lightning" streamers from laser induced cavities in phosphoric acid, in *Fortschritte der Akustik—DAGA 2020* (DEGA e.V., Berlin, 2020), pp. 413–416.

[37] B. C. Knott, J. L. LaRue, A. M. Wodtke, M. F. Doherty, and B. Peters, Communication: Bubbles, crystals, and laser-induced nucleation, J. Chem. Phys. (N.Y.) **134,** 171102 (2011).

[38] M. R. Ward, W. J. Jamieson, C. A. Leckey, and A. J. Alexander, Laser-induced nucleation of carbon dioxide bubbles, J. Chem. Phys. (N.Y.) **142,** 144501 (2015).

[39] U. Parlitz, V. Englisch, C. Scheffczyk, and W. Lauterborn, Bifurcation structure of bubble oscillators, J. Acoust. Soc. Am. **88,** 1061 (1990).

[40] D. Lohse and S. Hilgenfeldt, Inert gas accumulation in sonoluminescing bubbles, J. Chem. Phys. (N.Y.) **107,** 6986 (1997).

[41] C. D. Ohl and R. Ikink, Shock-Wave-Induced Jetting of Micron-Size Bubbles, Phys. Rev. Lett. **90,** 214502 (2003).

[42] I. Akhatov, R. Mettin, C. D. Ohl, U. Parlitz, and W. Lauterborn, Bjerknes force threshold for stable single bubble sonoluminescence, Phys. Rev. E **55,** 3747 (1997).

[43] T. Kurz, D. Kröninger, R. Geisler, and W. Lauterborn, Optic cavitation in an ultrasonic field, Phys. Rev. E **74,** 066307 (2006).

[44] J. Jin, R. Wang, J. Tang, L. Yang, Z. Feng, C. Xu, F. Yang, and N. Gu, Dynamic tracking of bulk nanobubbles from microbubbles shrinkage to collapse, Colloids Surf. A **589,** 124430 (2020).

[45] P. B. Duncan and D. Needham, Test of the Epstein-Plesset model for gas microparticle dissolution in aqueous media: Effect of surface tension and gas undersaturation in solution, Langmuir **20,** 2567 (2004).

[46] S. Ke, W. Xiao, N. Quan, Y. Dong, L. Zhang, and J. Hu, Formation and stability of bulk nanobubbles in different solutions, Langmuir **35,** 5250 (2019).

[47] W. Zhou, J. Zhang, L. Liu, and X. Cai, Ultrafast image-based dynamic light scattering for nanoparticle sizing, Rev. Sci. Instrum. **86,** 115107 (2015).